Palaeogeography, Palaeoclimatology, Palaeoecology 534 (2019) 109341

Contents lists available at ScienceDirect

Palaeogeography, Palaeoclimatology, Palaeoecology

journal homepage: www.elsevier.com/locate/palaeo

Did early land plants produce a stepwise change in atmospheric oxygen during the Late Ordovician (Sandbian ~458 Ma)?

Y. Datu Adiatma[a,*], Matthew R. Saltzman[a], Seth A. Young[b], Elizabeth M. Griffith[a], Nevin P. Kozik[b], Cole T. Edwards[c], Stephen A. Leslie[d], Alyssa M. Bancroft[e]

[a] School of Earth Sciences, The Ohio State University, Columbus, OH, USA
[b] Department of Earth, Ocean, and Atmospheric Science, National High Magnetic Field Laboratory, Florida State University, Tallahassee, FL, USA
[c] Department of Geological and Environmental Sciences, Appalachian State University, Boone, NC, USA
[d] Department of Geology and Environmental Science, James Madison University, Harrisonburg, VA, USA
[e] Indiana Geological and Water Survey, Indiana University, Bloomington, IN, USA

ARTICLE INFO

Keywords:
Carbon isotopes
Strontium isotopes
Chemostratigraphy
Oxygenation
Land plants
Appalachian Basin

ABSTRACT

A stepwise change in atmospheric oxygen (O_2) levels during the Ordovician has been attributed to the emergence of land plants. This phenomenon is tied to a major baseline shift in the stable carbon isotope ($\delta^{13}C$) curve and inferred increase in nutrient delivery and enhanced primary productivity in nearshore settings, which led to high organic carbon burial. The timing and magnitude of this baseline shift, however, is still elusive in part because of the lack of high-resolution $\delta^{13}C$ data that span this period. Much of the existing Ordovician $\delta^{13}C$ literature is focused on isotopic excursions with less emphasis on identifying long-term shifts in baseline (pre- and post-excursion) values.

This study presents new high resolution $\delta^{13}C$ data from stratigraphic sections at Germany Valley (West Virginia) and Union Furnace (Pennsylvania) in the Central Appalachian Basin. These sections span the entire Sandbian Stage and continue into the lower Katian Stage. The $\delta^{13}C$ data from both sections are characterized by relative stability carbon isotope values (mean = −0.61‰) in the lower Sandbian, followed by a + 1.2‰ shift in the upper Sandbian (mean = +0.62‰). Herein, we propose that the positive shift represents a long-term global shift in baseline $\delta^{13}C$ values of dissolved inorganic carbon. The timing of this positive shift coinciding with the diversification of early land plants (i.e., bryophytes) supports earlier models that suggested enhanced organic carbon burial rates served as a mechanism for the stepwise oxygenation of the atmosphere during the Late Ordovician.

1. Introduction

There is an important transition in Earth history during the Middle to Late Ordovician (470–443.8 Ma) that was marked by a three-fold increase in family level diversity, known as the Ordovician Radiation (Sepkoski, 1995) or the Great Ordovician Biodiversification Event (GOBE) (Webby, 2004; Servais and Harper, 2018; Stigall et al., 2019—this issue), that broadly coincided with the onset of global cooling (Trotter et al., 2008; Algeo et al., 2016; Rasmussen et al., 2016). Recent studies suggest that a major episode in the oxygenation of Earth's atmosphere may have taken place alongside these changes in climate and biodiversity (e.g., Lenton et al., 2016; Edwards, 2018; Krause et al., 2018). Rasmussen et al. (2019) and Stigall et al. (2019—this issue) have suggested that these observed changes in the Ordovician Earth system represent a critical transition that led to a planetary-scale biotic state shift (sensu Barnosky et al., 2012). This biotic and climatic shift may ultimately be tied to a fundamental shift in the global carbon cycle, which can be investigated in the geologic past by using the carbon isotopic ($\delta^{13}C$) composition of marine carbonate rocks.

Carbon isotope ($\delta^{13}C$) stratigraphy can be utilized to estimate fluctuations of carbon input and output fluxes to the ocean-atmosphere system (e.g., burial and weathering of carbonate and organic matter) in global carbon cycle models (Kump and Arthur, 1999; Berner, 2006; Royer et al., 2014). There are two distinct types of long term carbon cycle models that incorporate $\delta^{13}C$: GEOCARB (Berner and Kothavala, 2001; Berner, 2006; Royer et al., 2014; Krause et al., 2018; Zhang et al., 2018) and COPSE (Carbon-Oxygen-Phosphorus-Sulfur-Evolution)

* Corresponding author.
E-mail address: adiatma.1@osu.edu (Y.D. Adiatma).

https://doi.org/10.1016/j.palaeo.2019.109341
Received 31 January 2019; Received in revised form 19 August 2019; Accepted 19 August 2019
Available online 22 August 2019
0031-0182/

(Bergman et al., 2004; Lenton et al., 2018). Recent variations of these models have focused attention on the stepwise oxygenation of the Paleozoic atmosphere (Dahl et al., 2010; Lenton et al., 2016; Krause et al., 2018; Lenton et al., 2018; Zhang et al., 2018). In particular, a Middle to Upper Ordovician shift in $\delta^{13}C$ baseline values from ~ −1‰ to +1‰ has been tied to changes in terrestrial plant evolution that, in turn, drove increased nutrient fluxes to the oceans (Lenton et al., 2016). This nutrient influx likely enhanced primary productivity and increased the net amount of organic burial, along with an overall increase in carbon sequestration efficiency due to higher carbon to phosphorus molecular ratios (C:P) of terrestrial organic matter burial, and marked the beginning of a major rise in oxygen levels (Lenton et al., 2016; Edwards et al., 2017). However, the precise timing and magnitude of this transition in the long-term baseline $\delta^{13}C$ values is poorly constrained within the Middle to Upper Ordovician because of uncertainty in identifying global $\delta^{13}C$ signals and the age models used in published datasets. Most of the existing Ordovician $\delta^{13}C$ literature has focused on isotopic events (i.e., excursions) with less emphasis on identifying long-term shifts in baseline (pre- and post-excursion) values. The timing and magnitude of this $\delta^{13}C$ baseline shift is critical to the evaluation of the hypothesis of a land plant driver for the stepwise increase in oxygen levels (O_2), which ultimately must be compared to the fossil record of land plant evolution.

We tested the notion that a stepwise change in baseline $\delta^{13}C$ values during the Sandbian Stage is driven by the diversification of primitive land plants by presenting a new high-resolution dataset from the Central Appalachian Basin. This region contains several thick marine carbonate successions through the Middle to Upper Ordovician coinciding broadly with the proposed changes in land plant evolution and organic carbon burial. We use Sr isotope stratigraphy with new $^{87}Sr/^{86}Sr$ data to complement existing biostratigraphic data and independently correlate $\delta^{13}C$ trends.

The data show a shift in $\delta^{13}C$ during the Sandbian Age of the Late Ordovician that is subtle in terms of magnitude (−0.61‰ to +0.62‰) but is distinct from the surrounding larger and transient positive isotopic excursions (e.g., the Mid-Darriwilian (MDICE) and the Guttenberg (GICE) carbon isotope excursions) and may record a fundamental state shift in the long-term carbon cycle. Depending on which carbon cycle model is used, this change may signal the onset of an increase toward modern oxygen levels in the atmosphere. This increase in $\delta^{13}C$ baseline values may have been the result of multiple causal factors, including not just the origin and expansion of land plants that enhanced weathering and increased the C:P ratio of buried organic matter on land (Lenton et al., 2016), but also rising sea levels that increased the areal seafloor extent (Ronov et al., 1980) of organic C burial (Arthur et al., 1987), cooling (Trotter et al., 2008; Rasmussen et al., 2016) that enhanced nutrient upwelling (Pope and Steffen, 2003), or increased silicate weathering leading to higher riverine nutrient delivery to the global ocean and increased organic burial.

2. Geologic setting

During the Sandbian, (458.4–453 Ma (Cooper and Sadler, 2012)), most of the Laurentian paleocontinent was located in the tropics (Fig. 1A) (Jin et al., 2013; Scotese, 2014; Swanson-Hysell and Macdonald, 2017; Torsvik and Cocks, 2017), and was conducive to carbonate deposition along the continental margins, particularly in the Appalachian Basin (Read, 1980, 1982; Pope and Read, 1998; Brezinski et al., 2012). Ordovician strata in the Appalachian Basin also record the change in tectonic setting from a passive margin to a convergent (foreland) basin (Mussman and Read, 1986; Hatcher, 2010; Macdonald et al., 2017). This tectonic change was accompanied by the uplift of the Taconic Mountains in the southern margin of Laurentia (Rodgers, 1971; Ettensohn, 2008; Hatcher, 2010).

The Sandbian Stage in the Appalachian Basin (Fig. 1) is dominated by two major carbonate lithologies, peritidal to shallow subtidal mudstones that are traditionally referred to as Black River-type lithology (in reference to the expansive Black River Group of the northeastern USA) and subtidal packstone and grainstone that are traditionally referred to as Trenton-type lithology (Trenton Group) (Keith, 1988). The Black River-type lithology is broadly characterized as a warm water tropical type carbonate facies because it is dominated by carbonate mud, and a variety of carbonate grains of presumed warmer water origin (Holland and Patzkowsky, 1996). The Trenton-type lithology is characterized by less carbonate mud and dominated by bioclastic packstone and grainstone, as well as abundant phosphate and terrigenous silt and clay, and was referred to as a “temperate type” carbonate deposit (Holland and Patzkowsky, 1996). Age control in the Black River and Trenton-type lithologies in the Appalachian Basin is largely based on North American Midcontinent conodont biostratigraphy (Cooper and Sadler, 2012). Because many conodont taxa in the Sandbian interval represent long-ranging species that provide low resolution age constraints, Sr isotope stratigraphy has been shown to be an important tool for high resolution age constraints and correlation, due to the rapid change of seawater $^{87}Sr/^{86}Sr$ values during this interval (Saltzman et al., 2014).

The transition between Black River and Trenton-type carbonate facies has been attributed to a variety of factors. It may be due in part to a global greenhouse to icehouse transition, or a local nutrient increase from upwelling (Holland and Patzkowsky, 1996; Pope and Read, 1998; Pope and Steffen, 2003). However, Quinton et al. (2018) show no cooling trend associated with this change using the sea surface temperature proxy from oxygen isotopes of conodont apatite, inconsistent with a greenhouse to icehouse transition. Other factors contributing to the transition between Black River and Trenton-type carbonate facies may include an increase in water turbidity in the Appalachian Basin due to enhanced weathering related to the Taconic Orogeny (Young et al., 2009; Quinton et al., 2016) or enhanced weathering associated with land plant evolution (Lenton et al., 2016).

3. Methods

3.1. Stable isotopes ($\delta^{13}C$ and $\delta^{18}O$)

Samples for stable carbon and oxygen isotope analyses were collected in 0.5 to 3-m intervals at both Union Furnace and Germany Valley through the Sandbian and lower Katian strata (see Section 4.1 for detailed descriptions). Weathered surfaces were removed using a water-based diamond blade saw. Selected regions of the samples, preferably micrite, were drilled using a masonry drill bit to produce carbonate powders for stable isotopes analyses. Previous studies have shown that micrite can record primary marine $\delta^{13}C$ values in the absence of calcite fossil materials (e.g., brachiopod shells) (Kump et al., 1999; Ainsaar et al., 2010; Saltzman and Thomas, 2012; Edwards and Saltzman, 2014).

Isotopic analyses were conducted at the National High Magnetic Field Laboratory at Florida State University (FSU-NHMFL). Analyses were performed on a ThermoFinnigan Delta Plus XP mass spectrometer interfaced to a ThermoFinnigan Gas Bench II Autocarbonate device. Powdered samples between 0.1 and 0.3 mg were weighed and placed in vials and roasted in an oven at 70 °C for at least 12 h to remove water and volatile contaminants. Samples were flushed with He gas before being converted to CO_2 by reacting with anhydrous phosphoric acid for 24 h on the Gas Bench II Autocarbonate device. Isotope ratios were corrected for ^{17}O contribution (Craig, 1957), and reported in delta notation in per mil (‰) relative to Vienna Peedee Belemnite standard (VPDB). Data quality and calibrations were monitored by replicate analysis of the NBS-19 standard and internal standards. Internal FSU-NHMFL standards (and the corresponding $\delta^{13}C$ and $\delta^{18}O$ values, respectively) included in the analyses are ROY-CC (+0.67‰, −12.02‰), MB-CC (−10.5‰, −3.5‰), and PDA (−1.3‰, −5.34‰). Analytical precision of our reported $\delta^{13}C$ and $\delta^{18}O$ values are ± 0.05‰ and ±

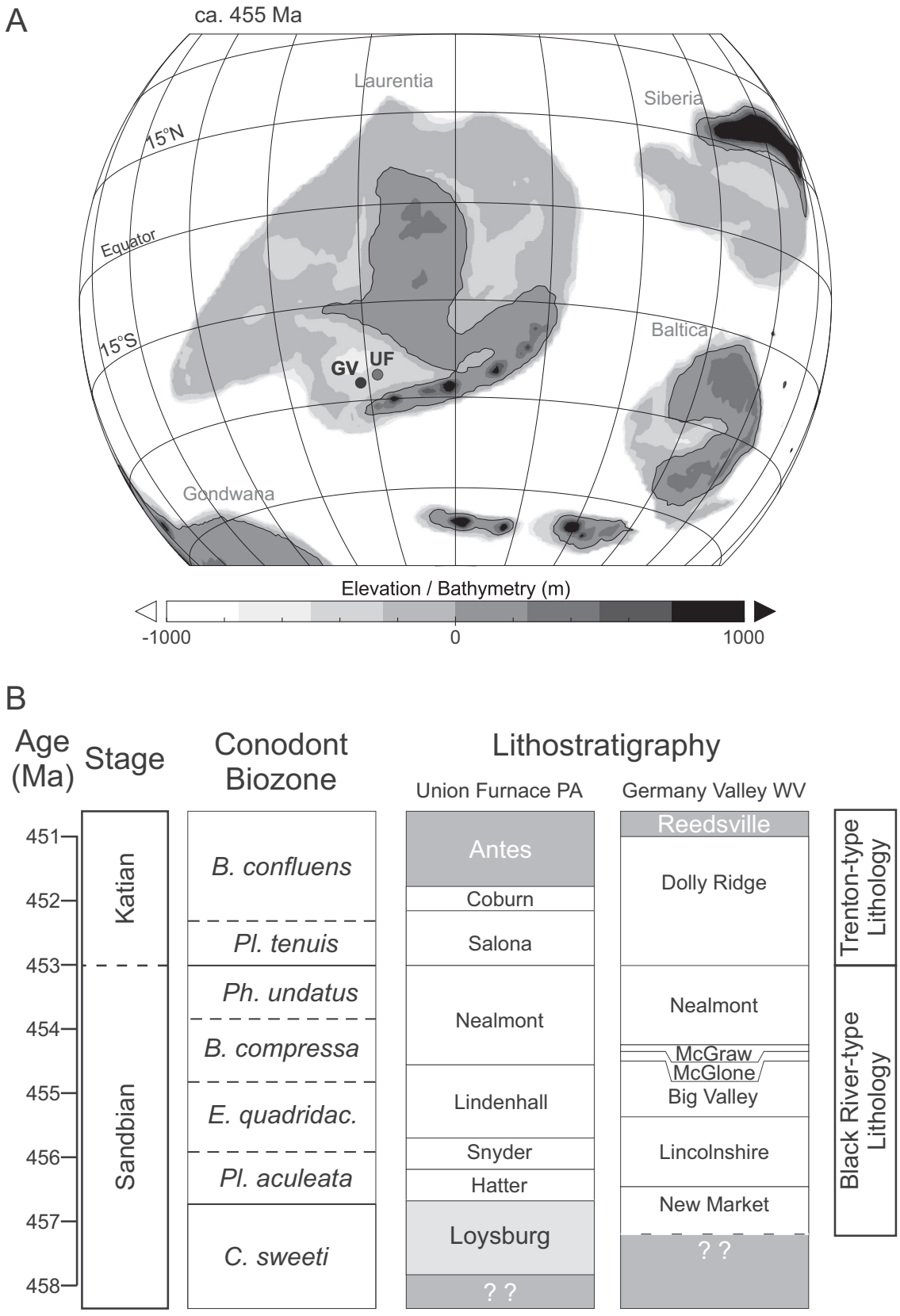

Fig. 1. Localities and lithostratigraphy. (A) Sampling localities at Germany Valley (GV), West Virginia and Union Furnace (UF), Pennsylvania, and paleogeographic map for the Late Ordovician (Sandbian) (Scotese and Wright, 2018). (B) Numerical ages and conodont biozones calibrated to the 2012 Geologic Time Scale (Cooper and Sadler, 2012). Oldest age shown represents the base of the Sandbian (top of Darriwilian). Age model for Union Furnace, PA is from Edwards et al. (2015) and Germany Valley, WV is based on Sr isotope curve presented herein and C isotope data of Young et al. (2005). See text for explanation of Black River- and Trenton-type lithology.

0.1‰, respectively.

3.2. Strontium isotopes ($^{87}Sr/^{86}Sr$)

Bulk rock carbonate powders were measured for their strontium isotopic value ($^{87}Sr/^{86}Sr$) as a proxy for seawater $^{87}Sr/^{86}Sr$ during the Sandbian. Previous studies suggest that bulk rock carbonate powders have the highest potential to faithfully record the $^{87}Sr/^{86}Sr$ value of seawater in the absence of fossil materials, if the samples come from rocks with low thermal maturity (determined independently from the Conodont Alteration Index (CAI)) or contain high Sr concentration (Montañez et al., 1996; Young et al., 2009; Li et al., 2011; Edwards et al., 2015).

Sample preparation followed the methods of Edwards et al. (2015). Carbonate powders for strontium isotope analyses were pre-treated with 1 M ammonium acetate (pH = 8), and leached with 4% acetic acid to remove contaminant radiogenic Sr (from clay minerals) or acid-soluble secondary Sr (e.g., recrystallized cement) (Montañez et al., 1996; Young et al., 2009; Li et al., 2011; Edwards et al., 2015). Leachates were spiked with an ^{84}Sr tracer to determine Sr concentrations using isotope dilution method, before being dried down on a hot plate overnight. Strontium purification was done using a cation exchange column method (modified from Foland and Allen (1991)). Dried down leachates were dissolved in 2N HCl and loaded onto 6 mL columns of BioRad AG50WX8 cation exchange resin and eluted with 2N ultrapure HCl. The total procedural blank was < 1% of the total recovered strontium which varied between 8 and 20 µg.

Strontium isotope ratios were measured on a Thermo Fisher Scientific TRITON Plus Thermal Ionization Mass Spectrometer (TIMS) at the Ohio State University Thermal Ionization Mass Spectrometry Laboratory. Samples were loaded on outgassed rhenium single filaments and measured with static collection mode. Previous studies in strontium isotope analyses (e.g., Foland and Allen, 1991) have suggested the importance of dynamic measurement (i.e., measuring ^{87}Sr and ^{86}Sr in the same faraday cup) to minimize faraday cup bias. In this study, however, we utilized the rotating virtual amplifier feature of the mass spectrometer, which minimizes bias in the faraday cups during measurement in the static mode. Isotopic ratios were normalized for fractionation during ionization and measurement using the natural Sr ratio of $^{86}Sr/^{88}Sr = 0.1194$ (Steiger and Jäger, 1977). The long-term value of NIST SRM 987 during measurement (January 2018–June 2018; $n = 44$) was $0.710243 \pm 8 \times 10^{-6}$ (2σ) with typical internal precision for each measurement (2σ) = 6×10^{-6}.

4. Results

4.1. Carbon isotope ($\delta^{13}C$) stratigraphy

4.1.1. Germany Valley section, West Virginia

The Germany Valley section, located in Riverton West Virginia, is a composite of two segments, the Arc Hollow section and the Dolly Ridge section of Young et al. (2005). The Germany Valley section contains the New Market, Lincolnshire, Big Valley, McGlone, McGraw, Nealmont, and Dolly Ridge formations, whereas the Dolly Ridge section contains the Nealmont and Dolly Ridge formations (Haynes et al., 2015). The segments, which are located within a quarter mile of each other, were correlated using formational boundaries and $\delta^{13}C$ chemostratigraphy.

The $\delta^{13}C$ record at the Germany Valley section, from base to top, begins with a decreasing trend from −0.2‰ to −0.4‰ within the New Market Formation, followed by a more gradual decreasing trend in the Lincolnshire Formation (Fig. 2). Relatively stable $\delta^{13}C$ values are recorded in the lower part of the Big Valley Formation followed by a 2.5‰ increase (from −1.2‰ to +1.3‰) in the upper part of the Big Valley Formation. Small-scale fluctuations, including a negative excursion spanning the McGlone and McGraw formations, are followed by an increasing trend across the Nealmont Formation. The $\delta^{13}C$ record ends with a relatively stable trend in the Nealmont Formation, followed by a 3.0‰ positive excursion spanning the Dolly Ridge Formation, previously identified at Dolly Ridge as the GICE (Young et al., 2005).

4.1.2. Union furnace section, central Pennsylvania

As with the Germany Valley section described above, the Union Furnace section is a composite of two segments, the main Union Furnace section, located along PA-453 in Tyrone Pennsylvania, and the previously published Reedsville section (Patzkowsky et al., 1997) located in Reedsville Pennsylvania (30 miles NE of the main section). The main Union Furnace section contains the Hatter, Snyder, Linden Hall, Nealmont, Salona, and Coburn formations, whereas the Reedsville section contains the Nealmont, Salona, and Coburn formations. These sections have been correlated using altered volcanic ash beds known as the Millbrig and Deicke K-Bentonites (Sell et al., 2013).

The $\delta^{13}C$ trend at the base of the Union Furnace section begins with decreasing values in the Hatter Formation from −0.6‰ to −1.8‰, followed by an increase to +0.3‰ at the lower part of Snyder Formation (Fig. 3). This increase is followed by an abrupt negative shift (1.0‰) within the Snyder Formation, followed by a steady increase from −1.3‰ to +1.3‰ in the Snyder Formation up to the middle part of the Nealmont Formation. The Sandbian record ends with a positive $\delta^{13}C$ excursion (identified as the GICE), which begins at the upper part of the Nealmont Formation and continues into the Coburn Formation (Fig. 3; Patzkowsky et al., 1997).

4.2. Strontium isotope ($^{87}Sr/^{86}Sr$) stratigraphy

Strontium isotope data measured from the Germany Valley section (Fig. 4) and published data from Union Furnace (Edwards et al., 2015) are used to constrain $\delta^{13}C$ correlations. New $^{87}Sr/^{86}Sr$ data are from the New Market Formation up to the lower part of the Dolly Ridge Formation. The samples from this section have Sr concentrations ranging from 255 to 943 ppm and CAI values of 4–4.5. The composite $^{87}Sr/^{86}Sr$ curve shows a general decreasing trend from 0.70845 at the New Market Formation to 0.70825 at the base of the Big Valley Formation, followed by more radiogenic and scattered values spanning the upper part of the Big Valley Formation to the base of the Dolly Ridge Formation (Fig. 4).

Whereas the general decreasing trend is broadly consistent with the seawater strontium isotope trend of the Middle to Upper Ordovician (Shields et al., 2003; Saltzman et al., 2014), the variability of values (~0.0003; Fig. 4) from the upper portion of the Germany Valley section (the upper part of Big Valley Formation to the lower part of Dolly Ridge Formation) indicates that these values may be altered, as generally observed for bulk rock analyses (e.g., Edwards et al., 2015). Previous studies have shown that thermal alteration can affect $^{87}Sr/^{86}Sr$ by incorporation of Sr through exchange with hydrothermal fluids (e.g., Bertram et al., 1992). However, thermal alteration alone cannot explain the difference in $^{87}Sr/^{86}Sr$ values between the lower and upper portion of the section (Fig. 4A). If thermal alteration was the sole agent that caused changes in primary Sr isotope signals, we would expect scattered values in the lower portion of the section as well. In addition, a previous study (Edwards et al., 2015) reported that samples with high CAI values, indicating high thermal alteration, can still preserve the primary seawater signal as long as the samples contain high enough Sr concentrations (> 300 ppm).

Herein, we propose that variations in carbonate lithology facilitated exchange of diagenetic fluids (evident by higher proportion of calcite veins) which, together with a higher proportion of clays, altered the primary Sr isotope signals in the upper portion of the section. A previous study by Holmden et al. (1996) argued that diagenetic fluids play a more significant role in Sr isotope ratio alteration regardless of CAI. The scattered isotope values in this study come from units that have more calcite veins (the upper Big Valley and the McGlone formations) or contain more abundant clay interbeds (Fig. 2; the Nealmont and

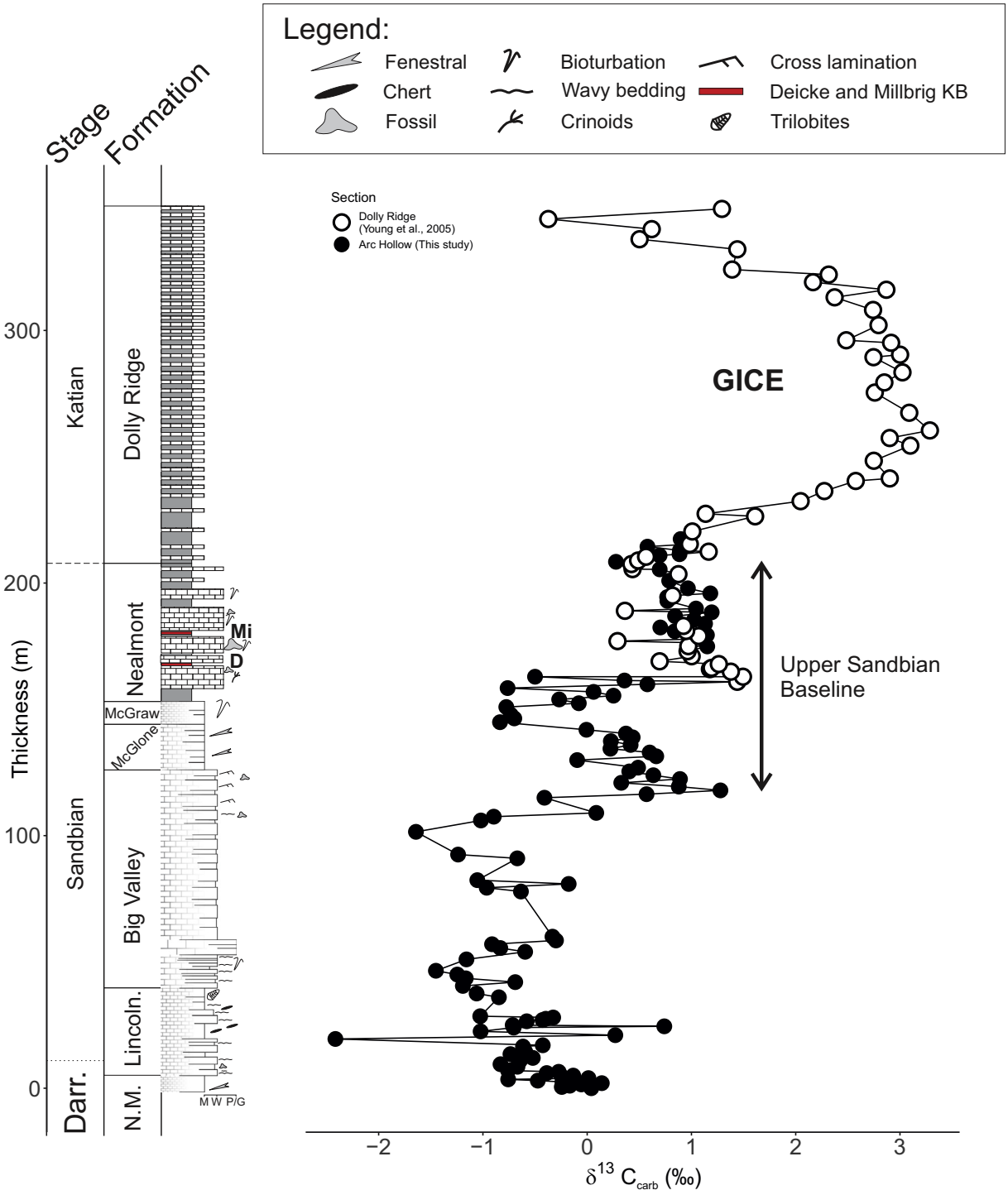

Fig. 2. Carbon isotope curve at Germany Valley, West Virginia. Correlation between the Arc Hollow (solid symbols, this study) and Dolly Ridge (open symbols, Young et al., 2005) segments in Germany Valley (separated by ~0.25 mile) is based on formational boundaries and overlapping of carbon isotope curves. M, W, P and G are mudstone, wackestone, packstone, and grainstone, respectively. Deicke (D) and Millbrig (Mi) K-bentonite (KB) are shown as red lines. (For interpretation of the references to colour in this figure legend, the reader is referred to the web version of this article.)

Dolly Ridge formations). Consequently, we only use $^{87}Sr/^{86}Sr$ values from the lower portion of the section (the New Market through lower part of Big Valley formations) to build a new age model for the Germany Valley section.

The new age model for the Germany Valley section was constructed using measured $^{87}Sr/^{86}Sr$ values calibrated to the global Ordovician seawater Sr curve (McArthur et al., 2012; Saltzman et al., 2014). Calibration curve construction follows the LOESS non-parametric local regression method (Cleveland and Devlin, 1988). In this study, we use the least altered values from the lower portion of the section and extrapolate to construct the seawater Sr curve (Fig. 4A). The upper portion of the constructed seawater curve is constrained by the seawater (LOESS) $^{87}Sr/^{86}Sr$ values for the base of the Katian from Saltzman et al. (2014) dataset (shown as black cross in Fig. 4A). The numerical age for the upper part of the section, which has altered $^{87}Sr/^{86}Sr$ values, was constrained using the published age for the GICE $\delta^{13}C$ excursion

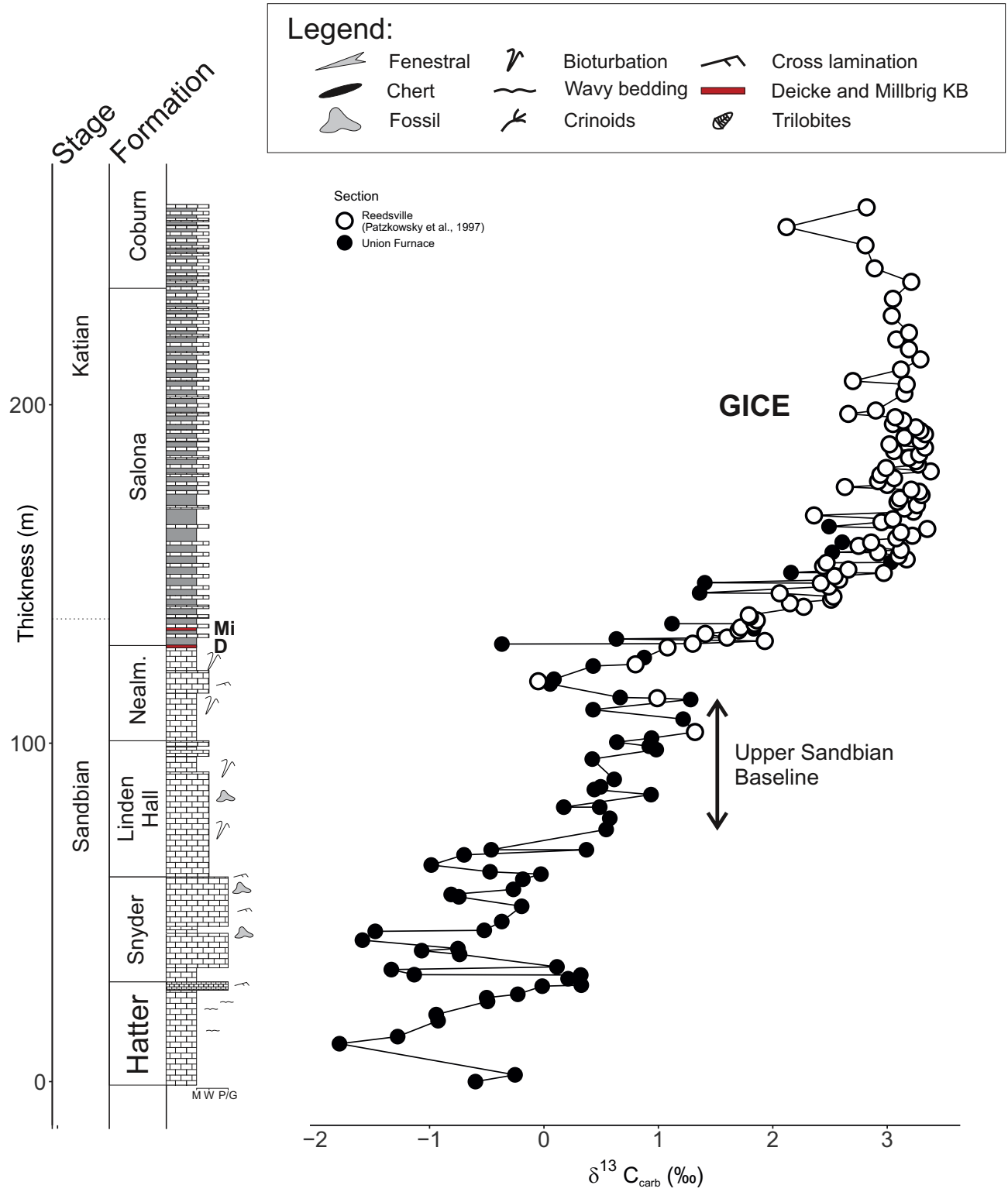

Fig. 3. Carbon isotope curve at Union Furnace, Pennsylvania. Open circles are from the Reedsville section in Patzkowsky et al. (1997) and closed circles are from this study. Correlation between the Union Furnace and Reedsville sections was done using K-Bentonite beds, formational boundaries, and carbon isotopes. M, W, P and G are mudstone, wackestone, packstone, and grainstone, respectively. Deicke (D) and Millbrig (Mi) K-bentonite (KB) are shown as red lines. (For interpretation of the references to colour in this figure legend, the reader is referred to the web version of this article.)

(Saltzman and Thomas, 2012). Further study in strontium isotope stratigraphy using conodont materials and high-resolution biostratigraphy is needed to better constrain the age model of the entire section. Nonetheless, we propose that the $\delta^{13}C$ curve from Germany Valley reported in this study covers the upper part of Darriwilian Stage, broadly coeval to the upper part of the *C. sweeti* Conodont Zone, the Sandbian Stage, and the lower Katian at the *Pl. tenuis* Conodont Zone, with numerical resolution of ± 0.7 Myr (based on the $^{87}Sr/^{86}Sr$ curve gradient, 95% confidence interval, and analytical precision of the calibration curve (i.e., Saltzman et al., 2014)).

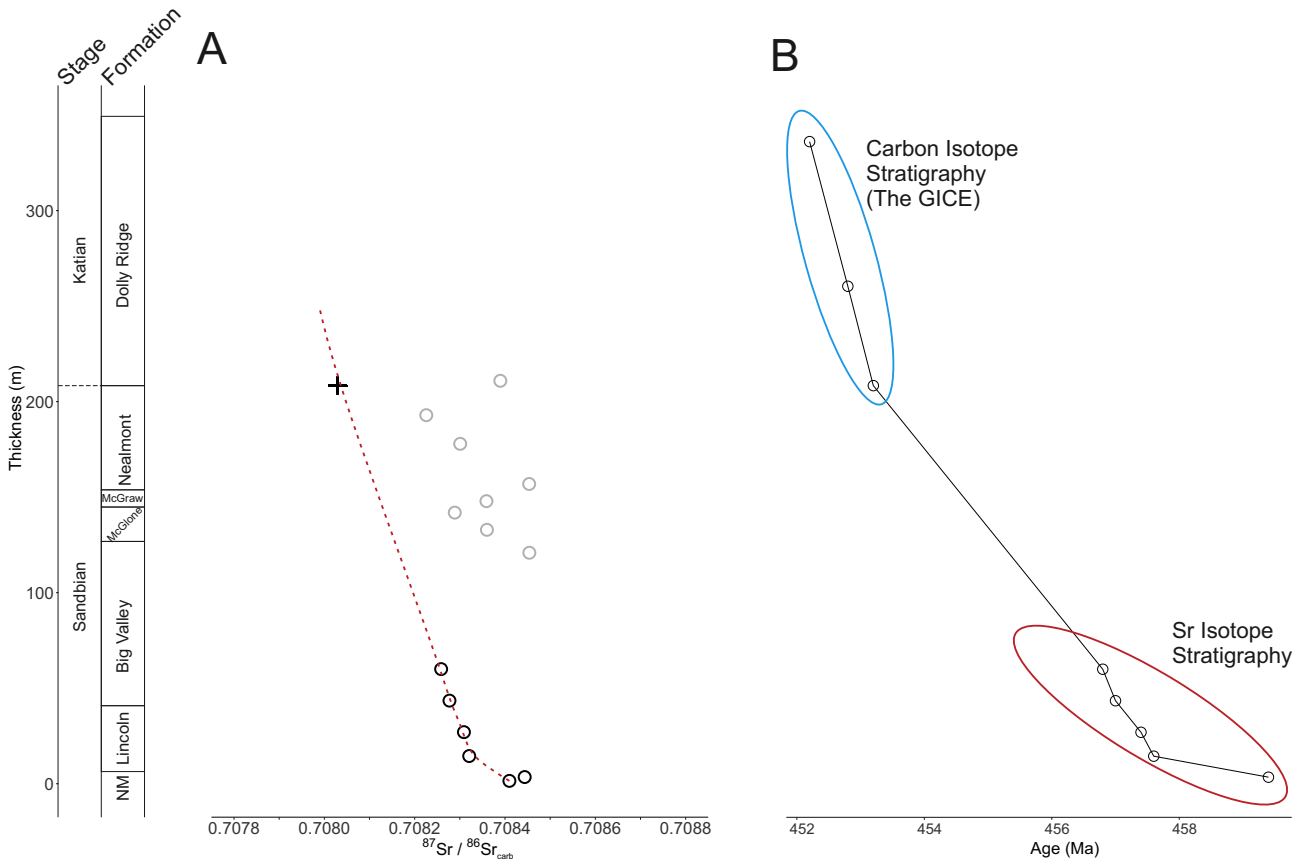

Fig. 4. Bulk-rock strontium isotope curve and age model of the Germany Valley, WV section based on chemostratigraphy. (A) Dashed red line is the proposed best fit to the seawater $^{87}Sr/^{86}Sr$ curve. The seawater trend is extrapolated using the seawater (LOESS) $^{87}Sr/^{86}Sr$ value for the base of the Katian Stage from Saltzman et al. (2014) (black cross), which is inferred using the onset of the GICE $\delta^{13}C$ excursion. (B) Age model was constructed using Sr isotope stratigraphy for lower portion (bottom 200 m) and carbon isotope stratigraphy (using the age of the GICE at the bottom, middle, and top of the excursion) (Young et al., 2005; Saltzman and Thomas, 2012) for the upper portion of the section.

5. Discussion

The construction of a continuous high-resolution $\delta^{13}C$ curve for the Sandbian, representing the marine dissolved inorganic carbon (DIC) pool, has implications for the timing and origin of a fundamental state change in the global carbon cycle that has been previously linked to the evolution of land plants (e.g., Lenton et al., 2016). Here we first evaluate any potential alteration of the global seawater signal in the measured $\delta^{13}C$ values, and then consider the origins of the $\delta^{13}C$ positive shift in the context of the oxygenation of the early Paleozoic oceans and atmosphere.

5.1. Primary seawater $\delta^{13}C$ signal preservation

Evaluating influences on the $\delta^{13}C$ signature of the measured bulk carbonate from the Appalachian Basin is important prior to using these data as a recorder of changes in the global carbon cycle. There are several processes that can decouple $\delta^{13}C$ values of carbonate rocks from the global DIC reservoir, such as isolation of isotopically distinct local water masses (Holmden et al., 1998) and restricted exchange with the open ocean (Patterson and Walter, 1994). In addition, preservation of $\delta^{13}C$ values might also be affected by alteration due to exchange with meteoric fluids (Banner and Hanson, 1990; Metzger and Fike, 2013).

A classic way to investigate diagenetic alteration of isotopic composition is by analyzing cross plots between $\delta^{13}C$ and $\delta^{18}O$. Covariation between $\delta^{13}C$ and $\delta^{18}O$ can indicate alteration of isotopic values in the carbonate rocks due to isotopic exchange between carbonate and porewater with distinct isotopic compositions (i.e., meteoric water) (e.g., Banner and Hanson, 1990). Cross plots between $\delta^{13}C$ and $\delta^{18}O$ from the Germany Valley and Union Furnace sections show no sign of covariation between $\delta^{18}O$ and $\delta^{13}C$ (Fig. 5), which suggests these samples are minimally altered.

Recent studies however, have questioned this method and argued that a covariation between $\delta^{13}C$ and $\delta^{18}O$ is a reflection of variable degree of recrystallization and neomorphism (Ahm et al., 2018; Swart and Oehlert, 2018), rather than mixing of isotopically distinct fluids within the sediments. Nevertheless, our chemostratigraphic correlations and comparison with other sections (see Section 5.2) indicates that the reported $\delta^{13}C$ data likely retain primary seawater signals. In addition, hand-sample descriptions of polished slabs (Fig. 6) show good preservation (e.g., minimal calcite veins, and signs of recrystallization), which supports the notion that primary $\delta^{13}C$ values are retained.

5.2. Sandbian $\delta^{13}C$ baseline shift

Correlation of $\delta^{13}C$ curves from across various paleocontinents shows that the Sandbian profiles from the central Appalachian Basin exhibit similar trends with profiles from the Great Basin and Baltoscandia (Fig. 7) (Saltzman and Young, 2005; Ainsaar et al., 2010; Saltzman and Edwards, 2017). Additionally, these general trends in Sandbian $\delta^{13}C$ values are documented in a recent study from the southern Appalachian Basin (Kozik et al., 2019). The Sandbian $\delta^{13}C$ trend begins with an interval of low $\delta^{13}C$ values (Sa1 Stage Slice of Bergström et al., 2009), which is known as the Kukruse Low in Baltoscandia (Ainsaar et al., 2010; Bergström et al., 2015). This low $\delta^{13}C$ interval is also well documented at the Antelope Range section in

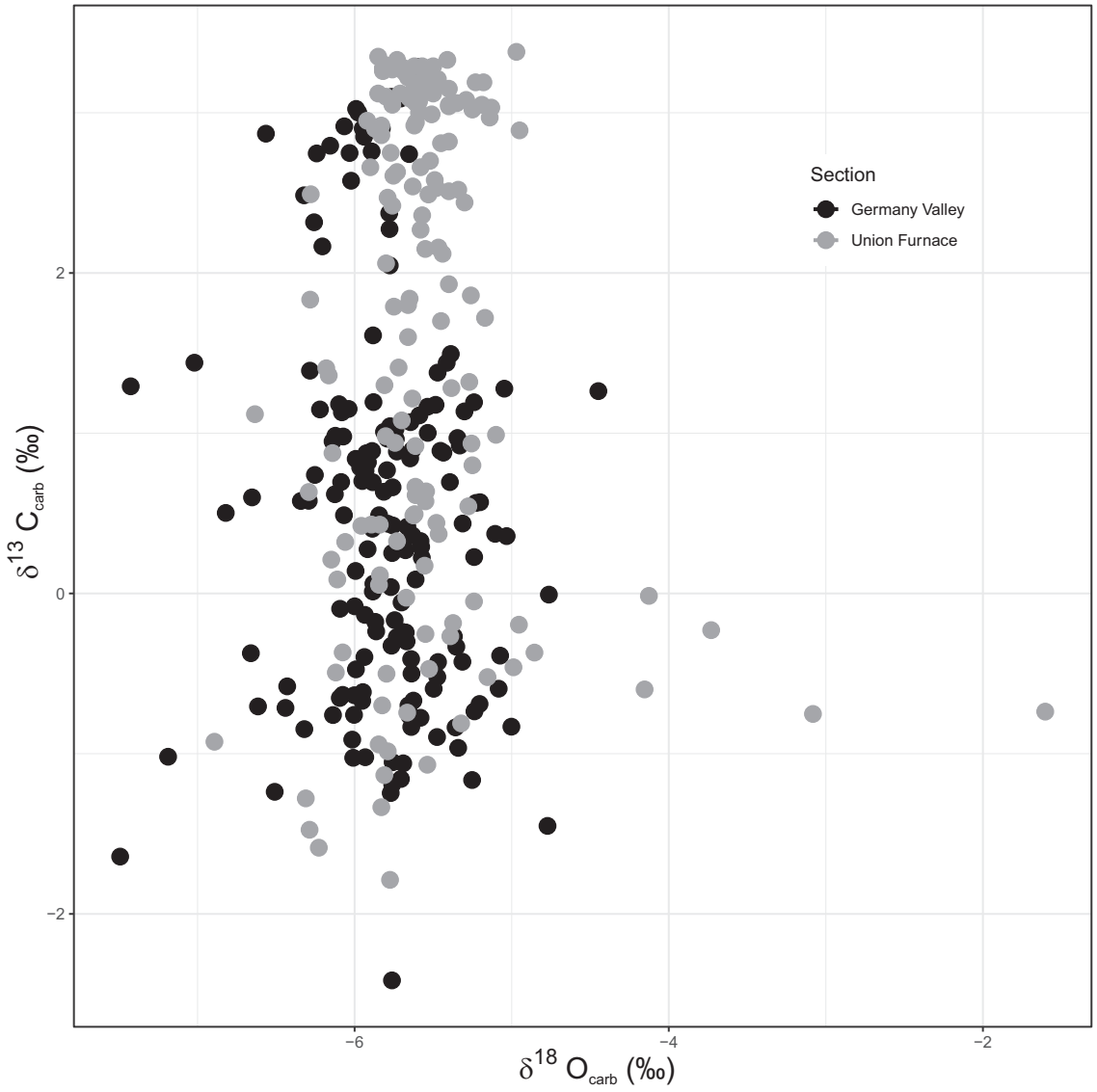

Fig. 5. Cross plot between $\delta^{13}C$ and $\delta^{18}O$ in permil relative to VPBD. Correlation coefficient between $\delta^{13}C$ and $\delta^{18}O$ (r^2) is −0.0088 (Germany Valley) and −0.0006 (Union Furnace) indicating a lack of correlation between $\delta^{18}O$ and $\delta^{13}C$ (see text for explanation).

Nevada and Clear Spring section in Maryland (Fig. 7). The Kukruse Low represents a minimum in $\delta^{13}C$ at the end of the declining limb of the MDICE. Although we cannot rule out that this $\delta^{13}C$ minimum (i.e., Kukruse Low) is a negative excursion between the MDICE and GICE, we instead interpret it to reflect a return to baseline values in between these positive excursions due to its relatively long duration (~2 Myr).

Though our sections are too young (i.e., Sandbian) to identify the MDICE or subsequent Kukruse Low, we interpret the lightest values in the Hatter Formation at Union Furnace and New Market – Lower Big Valley formations at Germany Valley as coeval event stratigraphic markers (possibly within the tail end of the Kukruse Low) (Figs. 2 and 3). The Kukruse Low is followed by a positive shift in $\delta^{13}C$ spanning most of the Sandbian interval. The magnitude of this positive shift is ~1.2 to 2‰ at the Antelope Range, Union Furnace, Germany Valley, and Kerguta sections, and 3‰ at the Clear Spring section (Fig. 7). The anomalously high-magnitude of the positive shift in the Clear Spring section is attributed to local amplification of $\delta^{13}C$, possibly due to increased carbonate platform restriction in this area of the Appalachian Basin (Saltzman and Edwards, 2017). The fact that this positive shift is observed in all sections supports the widespread and potentially global nature of this positive shift. In addition, a *t*-test was performed on the Germany Valley and Union Furnace $\delta^{13}C$ datasets (see supplementary material) and it suggests the baseline shift we observe is statistically significant.

We interpret this ≥1.2‰ positive shift observed in our studied sections as a long-term, stepwise change of the global $\delta^{13}C$ baseline. The positive shift observed in the Sandbian could alternatively be a short-lived carbon isotope excursion caused by a transient perturbation in the C cycle, such as a transient increase in organic matter burial due to an increase in productivity (Arthur et al., 1987; Kump and Arthur, 1999; Rasmussen et al., 2016) or an increase in isotopic values of riverine flux (Kump et al., 1999). However, the long duration (~2 Myr) and the fact that the Sandbian positive shift lacks a declining limb indicates that the positive shift marks a fundamental change in the steady state condition of the global marine DIC reservoir (Fig. 7). The Sandbian shift appears to represent the first time that positive $\delta^{13}C$ baseline values are maintained in the Paleozoic, following a period of lighter baseline values below 0‰ during the Cambrian to Early Ordovician interval (Fig. 8; Saltzman and Thomas, 2012; Lenton et al., 2016).

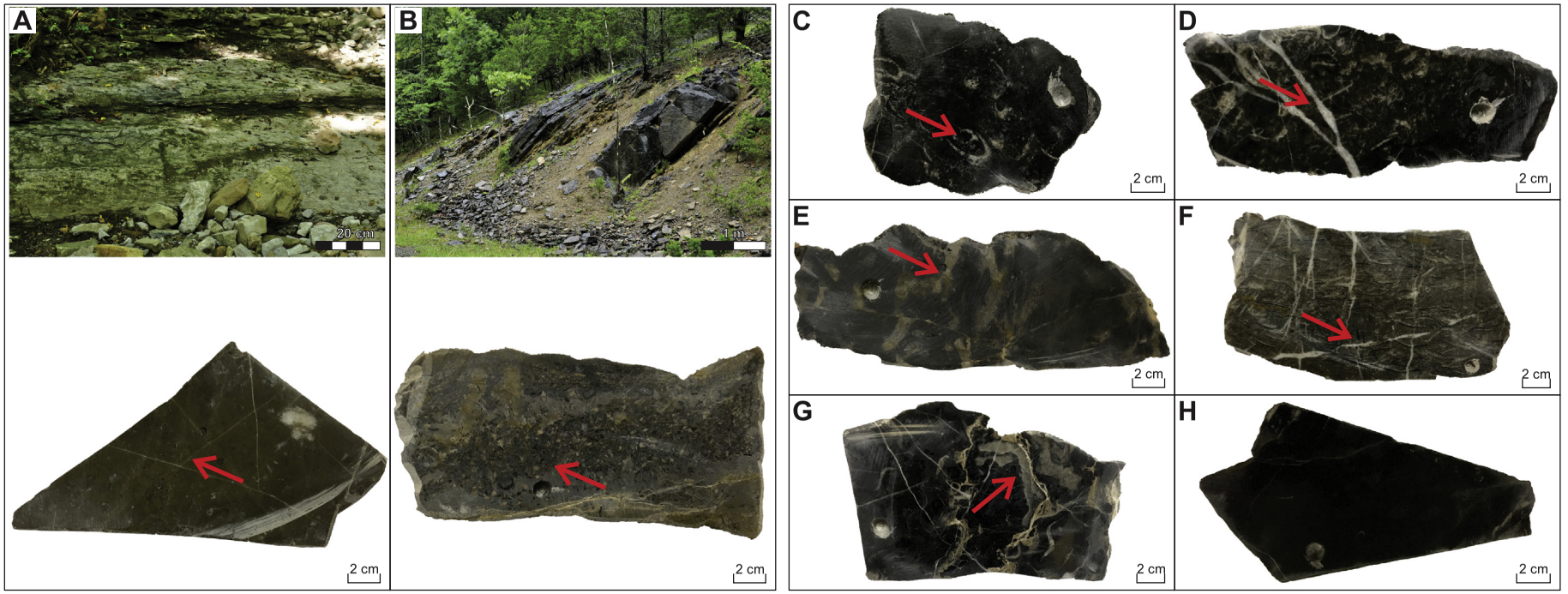

Fig. 6. Outcrop photos and polished slabs from Germany Valley, West Virginia. (A) Outcrop and polished slab of fenestral facies (arrow points to fenestrae) from the New Market Formation. (B) Outcrop and slab of fossiliferous grainstone facies from the Nealmont Formation (arrow points to burrow). The change in facies from the New Market to Nealmont formations indicates a general deepening trend. (C) Slab of fossiliferous (arrow) wackestone facies from the Big Valley Formation. (D) Calcite vein (arrow) within fossiliferous wackestone facies and (E) intense bioturbation (arrow) from the McGraw Formation. (F) Calcite vein (arrow) in grainstone facies of the Nealmont Formation. (G) Recrystallized burrow? (arrow) from the Big Valley Formation. (H) Micritic mudstone from the Lincolnshire Formation.

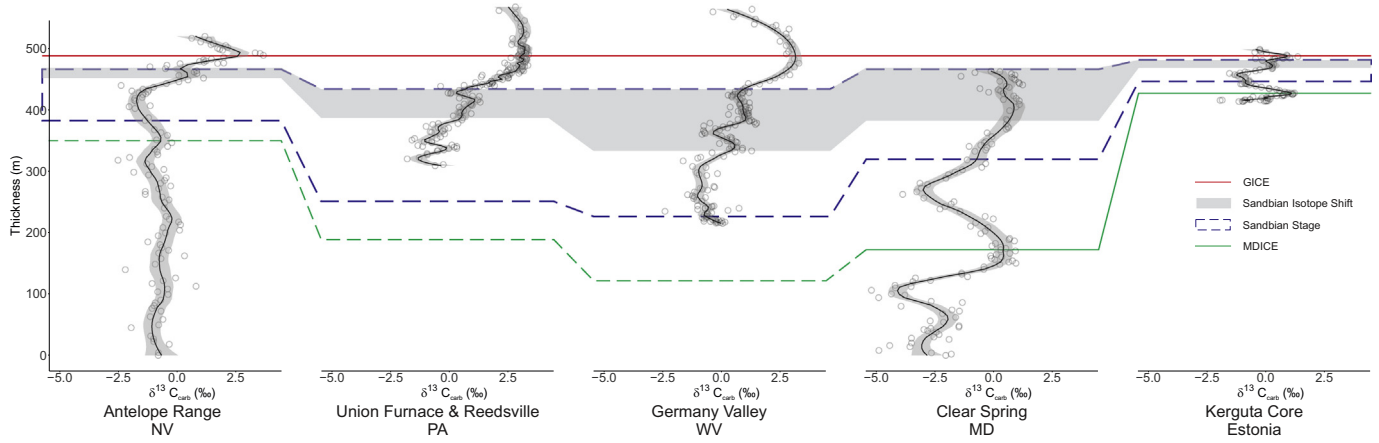

Fig. 7. Correlation of Late Ordovician $\delta^{13}C$ curves from different basins around the world. Antelope Range data are from Saltzman and Young (2005). Union Furnace and Reedsville composite section (this study and Patzkowsky et al. (1997)). Germany Valley composite section (this study and Young et al. (2005)). Clear Spring and Kerguta from Saltzman and Edwards (2017) and Ainsaar et al. (2010), respectively. Red and green lines correlate the peak of the GICE and MDICE, respectively. Blue dashed lines represent the lower and upper boundaries of the Sandbian Stage. Black curves in each section are drawn using LOESS (Cleveland and Devlin, 1988). Grey area marks the positive shift in baseline values during the Sandbian Stage interpreted as a global change associated with changes in land plant evolution. (For interpretation of the references to colour in this figure legend, the reader is referred to the web version of this article.)

5.3. Causes of $\delta^{13}C$ baseline shift in the Sandbian

One way to induce a shift in the steady state condition of the global DIC reservoir is by changing the isotopic composition of the riverine flux. Carbonate rocks, in general, tend to be more enriched in ^{13}C relative to organic matter. Therefore, an increase in carbonate weathering would shift the isotopic composition of the global riverine influx toward more positive values. The positive carbon isotope excursion in the Hirnantian Stage of the Ordovician, for instance, has been thought to be a consequence of an increase in the weathering of carbonate rocks due to eustatic sea-level fall (Kump et al., 1999). However, unlike the Hirnantian Stage in which a glacio-eustatic drop in sea level exposed carbonate platforms, the Sandbian Stage of the Upper Ordovician is characterized by overall rising (transgressive) of sea level (Haq and Schutter, 2008), following a regressive trend in the lower Darriwilian (e.g., Rasmussen et al., 2009, 2016).

Sea-level rise could also be a potential driver of a baseline shift in $\delta^{13}C$ during the Middle to Late Ordovician. In an ocean in which the location of deep water formation is in mid-latitudes (rather than high latitudes like today), a rise in sea level can cause an increase in the surface productivity due to expansion of shelf area and sinking deep water (warm saline bottom water) that enhanced nutrient upwelling (Arthur et al., 1987). This would lead to an increase in organic matter burial and preservation (if linked to an expansion of the oxygen minimum zones) (Arthur et al., 1987). This is consistent with the global long-term sea-level reconstructions for Middle to Late Ordovician (e.g., Haq and Schutter, 2008; Dronov, 2017). Field observations in the Appalachian Basin sections done for this study also suggest a general rise in relative sea level from shallow restricted facies of the New Market Formation to deeper marine facies in the Nealmont and Dolly Ridge formations (Fig. 6). However, in this scenario of a global sea-level rise as the driver of a baseline shift in $\delta^{13}C$ during the Sandbian, once eustatic sea level ultimately falls again the $\delta^{13}C$ baseline should return to its pre-shift values. This does not appear to be the case (Saltzman and Thomas, 2012) but instead Paleozoic sea-level reconstructions (Haq and Schutter, 2008 Fig. 8B) suggest a long-term sea-level fall (associated with the assembly of Pangea, see tectonic discussion below) from the end of the Ordovician to the Permian, inconsistent with a long-term positive shift in the $\delta^{13}C$ baseline.

The most probable explanation for the observed long-term shift in $\delta^{13}C$ baseline values is a unidirectional change in the global carbon cycle and Earth system, such as the rise and diversification of terrestrial non-vascular land plants in the Ordovician (Lenton et al., 2016; Porada et al., 2016). Previous studies, based on geochemical redox proxies (e.g., Wallace et al., 2017), and sedimentary charcoal deposits (Glasspool and Scott, 2010), have proposed a link between the emergence of large vascular land plants and an increase in atmospheric oxygen levels by the Devonian. An earlier role for non-vascular land plants in reshaping the carbon cycle and atmospheric oxygen is still an ongoing debate, partly due to the lack of geochemical (redox proxies) evidence and plant fossil records.

Previous studies have argued that non-vascular land plants are able to enhance silicate weathering, which in turn increases nutrient delivery (i.e., phosphorus) and invigorates organic matter burial (Lenton et al., 2012; Quirk et al., 2015; Lenton et al., 2016; Porada et al., 2016). Potential increases in silicate weathering flux (~2.8 km^3/yr) by non-vascular land plants and the corresponding terrestrial biomass (~133 Gt C) during the Late Ordovician have been estimated using simulated Net Primary Productivity (NPP) values and a global process-based vegetation model (Porada et al., 2013, 2016). This model translates NPP into silicate weathering flux by assuming that the flux is proportional to the required phosphorus for building up the terrestrial biomass (Porada et al., 2016). Moreover, experimental studies using modern bryophytes have suggested preferential weathering of phosphorus by non-vascular land plants (amplified by ~9- to 24-fold) compared to Ca and Mg (e.g., Lenton et al., 2012; Quirk et al., 2015). These findings support the NPP based weathering model and imply an increase in phosphorus delivery into the ocean during the Late Ordovician.

Although constraining the relative importance of non-vascular land plants in enhancing silicate weathering is not straightforward, in part because tectonics may also have played a role in enhanced weathering (Young et al., 2009; Swanson-Hysell and Macdonald, 2017), it is worth noting that a tectonic scenario requires an increase in carbonate weathering (Shields and Mills, 2017), which is difficult to constrain. Moreover, the abundance of phosphatic deposits in Upper Ordovician intervals (Pope and Steffen, 2003) might serve as evidence for an increase in the phosphorus flux during the Late Ordovician (Lenton et al., 2016). The abundance of phosphatic deposits and the positive baseline shift in the $\delta^{13}C$ curve are consistent with the hypothesis of non-vascular land plants as the driver for a permanent change in global carbon cycle and associated increase in atmospheric oxygen levels.

Additionally, the timing of this positive $\delta^{13}C$ shift is broadly correlated to a major evolutionary event in which mosses, hornworts, and proto-vascular plants diverged from liverworts (Kenrick et al., 2012)

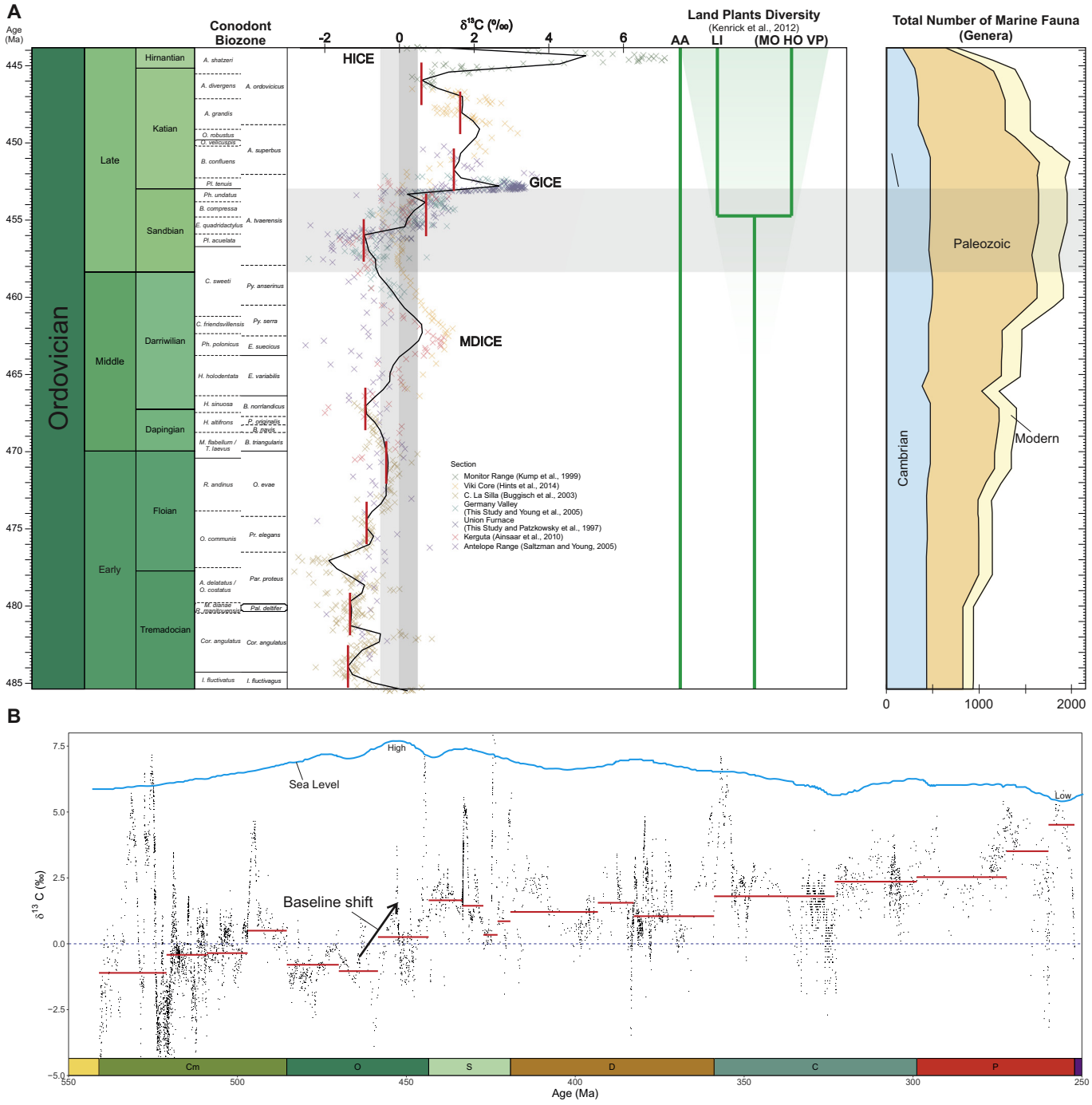

Fig. 8. $\delta^{13}C$ curve and biodiversity pattern across the Ordovician. (A) The positive shift of the $\delta^{13}C$ baseline value in the Sandbian (horizontal grey band) coincides with an increase in biodiversity of terrestrial plants based on Kenrick et al. (2012) and marine fauna genera (Sepkoski, 1995; Edwards et al., 2017; Servais and Harper, 2018). Composite $\delta^{13}C$ curve is constructed using data from Monitor Range (Kump et al., 1999), Viki core (Hints et al., 2014), C. La Sila (Buggisch et al., 2003), Kerguta (Ainsaar et al., 2010), Antelope Range (Saltzman and Young, 2005), Union Furnace (this study and Patzkowsky et al., 1997), and Germany Valley (this study and Young et al., 2005). AA, algal ancestor; LI, liverworts; MO, mosses; HO, hornworts; VP, vascular plants. Three well-known $\delta^{13}C$ excursions are known as the MDICE (Mid-Darriwilian), the GICE (Guttenberg) and the HICE (Hirnantian). Red lines are placed at points before and after excursions and are intended as schematic representation of the pre- and post- excursion baselines of the Ordovician $\delta^{13}C$. The smoothed curve was drawn using LOESS method. Vertical grey boxes highlight the baseline shift from negative values to positive values.
(B) Paleozoic baseline curve highlights the long-term significance of the Ordovician shift. Composite chemostratigraphic curve of Paleozoic δ13C data are compilation from Saltzman and Thomas (2012). The red horizontal lines are estimated baselines in Series level. Baselines are defined as the mean of $\delta^{13}C$ values that have rate of change < 0.5‰/Myr (i.e., stable). This figure shows a positive shift that took place during the Middle – Late Ordovician (see panel A for detailed view). Sea-level curve is from Haq and Schutter (2008). Abbreviation of geological periods: Cm, Cambrian; O, Ordovician; S, Silurian; D, Devonian; C, Carboniferous; P, Permian. Data are calibrated to Geologic Time Scale 2012 (Cooper and Sadler, 2012). (For interpretation of the references to colour in this figure legend, the reader is referred to the web version of this article.)

during the Sandbian (Fig. 8A). A comprehensive review by Kenrick et al. (2012) proposed a scenario of terrestrial colonization by land plants that began in the Middle Ordovician, followed by major evolutionary events (diversification of mosses, hornworts and proto-vascular plants from liverworts) during the Late Ordovician (Sandbian). The timing of this diversification is based on a molecular clock approach and has yet to be constrained with fossil evidence or biomarker data. It should also be noted that a recent study (Morris et al., 2018) places the emergence of the bryophytes somewhere within the Katian to the Mississippian, which represents a very large uncertainty of almost 100 million years.

The high-resolution trend of the Upper Ordovician $\delta^{13}C$ curve reported in this study suggests that the carbon cycle might have evolved in a stepwise fashion that is consistent with previous hypotheses of alternating ocean redox states during the Middle to Late Ordovician (Thompson and Kah, 2012; Jones and Fike, 2013; Young et al., 2016; Kozik et al., 2019). In contrast, previous modeling studies (Lenton et al., 2016; Krause et al., 2018) have suggested a relatively gradual increase of atmospheric oxygen level during the Middle to Late Ordovician. This debate mirrors the study of biological evolution during this time, in which recent studies show a stepwise (rather than gradual) change in the pattern of biotic evolution during the GOBE (Rasmussen et al., 2019). Although the debate over the timing and pattern of changes in the linked carbon and oxygen cycles must be addressed with additional multi-proxy datasets (including both $\delta^{13}C$ and redox proxies), we suggest that the presence and diversification of land plants fundamentally changed the carbon cycle, increasing the baseline $\delta^{13}C$ value of the global marine DIC reservoir throughout much of the remainder of the Phanerozoic.

6. Conclusions

This study set out to test the notion that a stepwise change in $\delta^{13}C$ during the Sandbian resulted from a permanent change in the carbon cycle related to the evolution of land plants. Our new high-resolution $\delta^{13}C$ data from the Central Appalachian Basin (Germany Valley and Union Furnace) reveals a ~1.2‰ positive shift in baseline values in bulk marine carbonates and confirm that this shift is global in extent based on inter-continental correlation. A new age model based on strontium isotope stratigraphy indicates that the positive $\delta^{13}C$ shift occurred during the late Sandbian. We argue that this represents a long-term baseline shift of marine DIC $\delta^{13}C$ values due to an increase in organic matter burial. The enhanced organic matter burial resulted from a change in weathering and carbon burial efficiency attributed to the presence and diversification of early land plants.

Acknowledgements

This study was supported by the Indonesia Endowment Fund for Education (LPDP), and the Friends of Orton Hall. Stable isotopes analyses were performed at the National High Magnetic Field Laboratory, which is supported by the National Science Foundation Cooperative Agreement No. DMR-1644779 and the State of Florida. Christopher Conwell, Teresa Avila, and Yodi Ramadhan helped with fieldworks and sample collections. Burt Wolff and Chelsie Bowman at FSU National High Magnetic Field Laboratory and Samantha Carter at OSU Thermal Ionization Mass Spectrometry Laboratory helped with isotopes analyses. We thank the Lambert family for granting us access to the Arc Hollow quarry. We thank Editor Thomas Algeo, Guest Editor Christian Rasmussen, Alycia Stigall, and two anonymous reviewers for insightful feedback that sharpened this manuscript.

Appendix A. Supplementary data

Supplementary data to this article can be found online at https://doi.org/10.1016/j.palaeo.2019.109341.

References

Ahm, A.-S.C., Bjerrum, C.J., Blättler, C.L., Swart, P.K., Higgins, J.A., 2018. Quantifying early marine diagenesis in shallow-water carbonate sediments. Geochim. Cosmochim. Acta 236, 140–159. https://doi.org/10.1016/j.gca.2018.02.042.

Ainsaar, L., Kaljo, D., Martma, T., Meidla, T., Männik, P., Nõlvak, J., Tinn, O., 2010. Middle and Upper Ordovician carbon isotope chemostratigraphy in Baltoscandia: a correlation standard and clues to environmental history. Palaeogeogr. Palaeoclimatol. Palaeoecol. 294, 189–201. https://doi.org/10.1016/j.palaeo.2010.01.003.

Algeo, T.J., Marenco, P.J., Saltzman, M.R., 2016. Co-evolution of oceans, climate, and the biosphere during the 'Ordovician Revolution': a review. Palaeogeogr. Palaeoclimatol. Palaeoecol. 458, 1–11. https://doi.org/10.1016/j.palaeo.2016.05.015.

Arthur, M.A., Schlanger, S.O., Jenkyns, H.C., 1987. The Cenomanian-Turonian oceanic anoxic event, II. Palaeoceanographic controls on organic-matter production and preservation. Geol. Soc. Lond. Spec. Publ. 26, 401–420. https://doi.org/10.1144/GSL.SP.1987.026.01.25.

Banner, J.L., Hanson, G.N., 1990. Calculation of simultaneous isotopic and trace element variations during water-rock interaction with applications to carbonate diagenesis. Geochim. Cosmochim. Acta 54, 3123–3137. https://doi.org/10.1016/0016-7037(90)90128-8.

Barnosky, A.D., Hadly, E.A., Bascompte, J., Berlow, E.L., Brown, J.H., Fortelius, M., Getz, W.M., Harte, J., Hastings, A., Marquet, P.A., Martinez, N.D., Mooers, A., Roopnarine, P., Vermeij, G., Williams, J.W., Gillespie, R., Kitzes, J., Marshall, C., Matzke, N., Mindell, D.P., Revilla, E., Smith, A.B., 2012. Approaching a state shift in Earth's biosphere. Nature 486, 52–58. https://doi.org/10.1038/nature11018.

Bergman, N.M., Lenton, T.M., Watson, A.J., 2004. COPSE: a new model of biogeochemical cycling over Phanerozoic time. Am. J. Sci. 304, 397–437. https://doi.org/10.2475/ajs.304.5.397.

Bergström, S.M., Chen, X., Gutiérrez-Marco, J.C., Dronov, A., 2009. The new chronostratigraphic classification of the Ordovician System and its relations to major regional series and stages and to $\delta^{13}C$ chemostratigraphy. Lethaia 42, 97–107. https://doi.org/10.1111/j.1502-3931.2008.00136.x.

Bergström, S.M., Saltzman, M.R., Leslie, S.A., Ferretti, A., Young, S.A., 2015. Trans-Atlantic application of the Baltic Middle and Upper Ordovician carbon isotope zonation. Est. J. Earth Sci. 64, 8. https://doi.org/10.3176/earth.2015.02.

Berner, R.A., 2006. Inclusion of the weathering of volcanic rocks in the GEOCARBSULF model. Am. J. Sci. 306, 295–302. https://doi.org/10.2475/05.2006.01.

Berner, R.A., Kothavala, Z., 2001. Geocarb III: a revised model of atmospheric CO_2 over Phanerozoic time. Am. J. Sci. 301, 182–204. https://doi.org/10.2475/ajs.301.2.182.

Bertram, C.J., Elderfield, H., Aldridge, R.J., Conway Morris, S., 1992. $^{87}Sr/^{86}Sr$, $^{143}Nd/^{144}Nd$ and REEs in Silurian phosphatic fossils. Earth Planet. Sci. Lett. 113, 239–249. https://doi.org/10.1016/0012-821X(92)90222-H.

Brezinski, D.K., Taylor, J.F., Repetski, J.E., 2012. Sequential development of platform to off-platform facies of the Great American Carbonate Bank in the Central Appalachians. In: Derby, J.R., Fritz, R.D., Longacre, S.A., Morgan, W.A., Sternbach, C.A. (Eds.), The Great American Carbonate Bank: The Geology and Economic Resources of the Cambrian-Ordovician Sauk Megasequence of Laurentia. AAPG Memoir, pp. 383–420.

Buggisch, W., Keller, M., Lehnert, O., 2003. Carbon isotope record of Late Cambrian to Early Ordovician carbonates of the Argentine Precordillera. Palaeogeogr. Palaeoclimatol. Palaeoecol. 195, 357–373. https://doi.org/10.1016/S0031-0182(03)00365-1.

Cleveland, W.S., Devlin, S.J., 1988. Locally weighted regression: an approach to regression analysis by local fitting. J. Am. Stat. Assoc. 83, 596–610. https://doi.org/10.1080/01621459.1988.10478639.

Cooper, R.A., Sadler, P.M., 2012. Chapter 20 - the Ordovician Period. In: The Geologic Time Scale. Elsevier, Boston, pp. 489–523. https://doi.org/10.1016/B978-0-444-59425-9.00020-2.

Craig, H., 1957. Isotopic standards for carbon and oxygen and correction factors for mass-spectrometric analysis of carbon dioxide. Geochim. Cosmochim. Acta 12, 133–149. https://doi.org/10.1016/0016-7037(57)90024-8.

Dahl, T.W., Hammarlund, E.U., Anbar, A.D., Bond, D.P.G., Gill, B.C., Gordon, G.W., Knoll, A.H., Nielsen, A.T., Schovsbo, N.H., Canfield, D.E., 2010. Devonian rise in atmospheric oxygen correlated to the radiations of terrestrial plants and large predatory fish. Proc. Natl. Acad. Sci. 107, 17911–17915. https://doi.org/10.1073/pnas.1011287107.

Dronov, A., 2017. Chapter five - Ordovician sequence stratigraphy of the Siberian and Russian platforms. In: Montenari, M. (Ed.), Stratigraphy & Timescales, Advances in Sequence Stratigraphy. Academic Press, pp. 187–241. https://doi.org/10.1016/bs.sats.2017.07.005.

Edwards, C.T., 2018. Links Between Early Paleozoic Oxygenation and the Great Ordovician Biodiversification. A review. Palaeoworld, Event (GOBE). https://doi.org/10.1016/j.palwor.2018.08.006.

Edwards, C.T., Saltzman, M.R., 2014. Carbon isotope (δ13Ccarb) stratigraphy of the Lower–Middle Ordovician (Tremadocian–Darriwilian) in the Great Basin, western United States: implications for global correlation. Palaeogeogr. Palaeoclimatol. Palaeoecol. 399, 1–20. https://doi.org/10.1016/j.palaeo.2014.02.005.

Edwards, C.T., Saltzman, M.R., Leslie, S.A., Bergström, S.M., Sedlacek, A.R.C., Howard, A., Bauer, J.A., Sweet, W.C., Young, S.A., 2015. Strontium isotope ($^{87}Sr/^{86}$ Sr) stratigraphy of Ordovician bulk carbonate: implications for preservation of primary seawater values. Geol. Soc. Am. Bull. 127, 1275–1289. https://doi.org/10.1130/B31149.1.

Edwards, C.T., Saltzman, M.R., Royer, D.L., Fike, D.A., 2017. Oxygenation as a driver of the Great Ordovician biodiversification event. Nat. Geosci. 10, 925–929. https://doi.

org/10.1038/s41561-017-0006-3.
Ettensohn, F.R., 2008. Chapter 4 the Appalachian foreland basin in Eastern United States. In: Sedimentary Basins of the World. Elsevier, pp. 105–179.
Foland, K.A., Allen, J.C., 1991. Magma sources for Mesozoic anorogenic granites of the White Mountain magma series, New England, USA. Contrib. Mineral. Petrol. 109, 195–211.
Glasspool, I.J., Scott, A.C., 2010. Phanerozoic concentrations of atmospheric oxygen reconstructed from sedimentary charcoal. Nat. Geosci. 3, 627–630. https://doi.org/10.1038/ngeo923.
Haq, B.U., Schutter, S.R., 2008. A chronology of Paleozoic sea-level changes. Science 322, 64–68. https://doi.org/10.1126/science.1161648.
Hatcher, R.D., 2010. The Appalachian orogen: a brief summary. In: Tollo, R.P., Bartholomew, M.J., Hibbard, J.P., Karabinos, P.M. (Eds.), From Rodinia to Pangea: The Lithotectonic Record of the Appalachian Region. Geological Society of America Memoirs, pp. 1–19.
Haynes, J.T., Goggin, K.E., Orndorff, R.C., Goggin, L.R., 2015. Ordovician of Germany Valley, West Virginia. IUGS, West Virginia.
Hints, O., Martma, T., Männik, P., Nõlvak, J., Põldvere, A., Shen, Y., Viira, V., 2014. New data on Ordovician stable isotope record and conodont biostratigraphy from the Viki reference drill core, Saaremaa Island, western Estonia. GFF 136, 100–104. https://doi.org/10.1080/11035897.2013.873989.
Holland, S.M., Patzkowsky, M.E., 1996. Sequence stratigraphy and long-term paleoceanographic change in the Middle and Upper Ordovician of the eastern United States. Geol. Soc. Am. Spec. Pap. 306, 117–129. https://doi.org/10.1130/0-8137-2306-X.117.
Holmden, C., Creaser, R.A., Muehlenbachs, K., Bergstrom, S.M., Leslie, S.A., 1996. Isotopic and elemental systematics of Sr and Nd in 454 Ma biogenic apatites: implications for paleoseawater studies. Earth Planet. Sci. Lett. 142, 425–437. https://doi.org/10.1016/0012-821X(96)00119-7.
Holmden, C., Creaser, R.A., Muehlenbachs, K., Leslie, S.A., Bergström, S.M., 1998. Isotopic evidence for geochemical decoupling between ancient epeiric seas and bordering oceans: Implications for secular curves. Geology 26, 567–570. https://doi.org/10.1130/0091-7613(1998)026<0567:IEFGDB>2.3.CO;2.
Jin, J., Harper, D.A.T., Cocks, L.R.M., McCausland, P.J.A., Rasmussen, C.M.Ø., Sheehan, P.M., 2013. Precisely locating the Ordovician equator in Laurentia. Geology 41, 107–110. https://doi.org/10.1130/G33688.1.
Jones, D.S., Fike, D.A., 2013. Dynamic sulfur and carbon cycling through the end-Ordovician extinction revealed by paired sulfate–pyrite $\delta^{34}S$. Earth Planet. Sci. Lett. 363, 144–155. https://doi.org/10.1016/j.epsl.2012.12.015.
Keith, B.D., 1988. Regional facies of upper Ordovician series of Eastern North America. In: Keith, B.D. (Ed.), The Trenton Group (Upper Ordovician Series) of Eastern North America: Deposition, Diagenesis, and Petroleum, AAPG Studies in Geology. American Association of Petroleum Geologists, pp. 1–16.
Kenrick, P., Wellman, C.H., Schneider, H., Edgecombe, G.D., 2012. A timeline for terrestrialization: consequences for the carbon cycle in the Palaeozoic. Philos. Trans. R. Soc., B 367, 519–536. https://doi.org/10.1098/rstb.2011.0271.
Kozik, N.P., Young, S.A., Bowman, C.N., Saltzman, M.R., Them, T.R., 2019. Middle–Upper Ordovician (Darriwilian–Sandbian) paired carbon and sulfur isotope stratigraphy from the Appalachian Basin, USA: implications for dynamic redox conditions spanning the peak of the Great Ordovician biodiversification event. Palaeogeogr. Palaeoclimatol. Palaeoecol. 520, 188–202. https://doi.org/10.1016/j.palaeo.2019.01.032.
Krause, A.J., Mills, B.J.W., Zhang, S., Planavsky, N.J., Lenton, T.M., Poulton, S.W., 2018. Stepwise oxygenation of the Paleozoic atmosphere. Nat. Commun. 9. https://doi.org/10.1038/s41467-018-06383-y.
Kump, L.R., Arthur, M.A., 1999. Interpreting carbon-isotope excursions: carbonates and organic matter. Chem. Geol. 161, 181–198. https://doi.org/10.1016/S0009-2541(99)00086-8.
Kump, L.R., Arthur, M.A., Patzkowsky, M.E., Gibbs, M.T., Pinkus, D.S., Sheehan, P.M., 1999. A weathering hypothesis for glaciation at high atmospheric pCO_2 during the Late Ordovician. Palaeogeogr. Palaeoclimatol. Palaeoecol. 152, 173–187. https://doi.org/10.1016/S0031-0182(99)00046-2.
Lenton, T.M., Crouch, M., Johnson, M., Pires, N., Dolan, L., 2012. First plants cooled the Ordovician. Nat. Geosci. 5, 86–89. https://doi.org/10.1038/ngeo1390.
Lenton, T.M., Dahl, T.W., Daines, S.J., Mills, B.J.W., Ozaki, K., Saltzman, M.R., Porada, P., 2016. Earliest land plants created modern levels of atmospheric oxygen. Proc. Natl. Acad. Sci. 113, 9704–9709. https://doi.org/10.1073/pnas.1604787113.
Lenton, T.M., Daines, S.J., Mills, B.J.W., 2018. COPSE reloaded: an improved model of biogeochemical cycling over Phanerozoic time. Earth-Sci. Rev. 178, 1–28. https://doi.org/10.1016/j.earscirev.2017.12.004.
Li, D., Shields-Zhou, G.A., Ling, H.-F., Thirlwall, M., 2011. Dissolution methods for strontium isotope stratigraphy: guidelines for the use of bulk carbonate and phosphorite rocks. Chem. Geol. 290, 133–144. https://doi.org/10.1016/j.chemgeo.2011.09.004.
Macdonald, F.A., Karabinos, P.M., Crowley, J.L., Hodgin, E.B., Crockford, P.W., Delano, J.W., 2017. Bridging the gap between the foreland and hinterland II: geochronology and tectonic setting of Ordovician magmatism and basin formation on the Laurentian margin of New England and Newfoundland. Am. J. Sci. 317, 555–596. https://doi.org/10.2475/05.2017.02.
McArthur, J.M., Howarth, R.J., Shields, G.A., 2012. Strontium isotope stratigraphy. In: The Geologic Time Scale. Elsevier, pp. 127–144. https://doi.org/10.1016/B978-0-444-59425-9.00007-X.
Metzger, J.G., Fike, D.A., 2013. Techniques for assessing spatial heterogeneity of carbonate $\delta^{13}C$ values: implications for craton-wide isotope gradients. Sedimentology 60, 1405–1431. https://doi.org/10.1111/sed.12033.
Montañez, I.P., Banner, J.L., Osleger, D.A., Borg, L.E., Bosserman, P.J., 1996. Integrated Sr isotope variations and sea-level history of Middle to Upper Cambrian platform carbonates: implications for the evolution of Cambrian seawater $^{87}Sr/^{86}Sr$. Geology 24, 917–920. https://doi.org/10.1130/0091-7613(1996)024<0917:ISIVAS>2.3.CO;2.
Morris, J.L., Puttick, M.N., Clark, J.W., Edwards, D., Kenrick, P., Pressel, S., Wellman, C.H., Yang, Z., Schneider, H., Donoghue, P.C.J., 2018. The timescale of early land plant evolution. Proc. Natl. Acad. Sci. 115, E2274–E2283. https://doi.org/10.1073/pnas.1719588115.
Mussman, W.J., Read, J.F., 1986. Sedimentology and development of a passive-to convergent-margin unconformity: middle Ordovician Knox unconformity, Virginia Appalachians. Geol. Soc. Am. Bull. 97, 282–295.
Patterson, W.P., Walter, L.M., 1994. Depletion of ^{13}C in seawater ΣC02 on modern carbonate platforms: significance for the carbon isotopic record of carbonates. Geology 22, 885–888. https://doi.org/10.1130/0091-7613(1994)022<0885:DOCISC>2.3.CO;2.
Patzkowsky, M.E., Slupik, L.M., Arthur, M.A., Pancost, R.D., Freeman, K.H., 1997. Late Middle Ordovician environmental change and extinction: harbinger of the Late Ordovician or continuation of Cambrian patterns? Geology 25, 911–914.
Pope, M., Read, J.F., 1998. Ordovician metre-scale cycles: implications for climate and eustatic fluctuations in the central Appalachians during a global greenhouse, non-glacial to glacial transition. Palaeogeogr. Palaeoclimatol. Palaeoecol. 138, 27–42. https://doi.org/10.1016/S0031-0182(97)00130-2.
Pope, M.C., Steffen, J.B., 2003. Widespread, prolonged late Middle to Late Ordovician upwelling in North America: a proxy record of glaciation? Geology 31, 63. https://doi.org/10.1130/0091-7613(2003)031<0063:WPLMTL>2.0.CO;2.
Porada, P., Weber, B., Elbert, W., Pöschl, U., Kleidon, A., 2013. Estimating global carbon uptake by lichens and bryophytes with a process-based model. Biogeosciences 10, 6989–7033. https://doi.org/10.5194/bg-10-6989-2013.
Porada, P., Lenton, T.M., Pohl, A., Weber, B., Mander, L., Donnadieu, Y., Beer, C., Pöschl, U., Kleidon, A., 2016. High potential for weathering and climate effects of non-vascular vegetation in the Late Ordovician. Nat. Commun. 7, 12113. https://doi.org/10.1038/ncomms12113.
Quinton, P.C., Herrmann, A.D., Leslie, S.A., MacLeod, K.G., 2016. Carbon cycling across the southern margin of Laurentia during the Late Ordovician. Palaeogeogr. Palaeoclimatol. Palaeoecol. 458, 63–76. https://doi.org/10.1016/j.palaeo.2015.08.020.
Quinton, P.C., Law, S., Macleod, K.G., Herrmann, A.D., Haynes, J.T., Leslie, S.A., 2018. Testing the early Late Ordovician cool-water hypothesis with oxygen isotopes from conodont apatite. Geol. Mag. 155, 1727–1741. https://doi.org/10.1017/S0016756817000589.
Quirk, J., Leake, J.R., Johnson, D.A., Taylor, L.L., Saccone, L., Beerling, D.J., 2015. Constraining the role of early land plants in Palaeozoic weathering and global cooling. Proc. R. Soc. B Biol. Sci. 282, 20151115. https://doi.org/10.1098/rspb.2015.1115.
Rasmussen, C.M.Ø., Nielsen, A.T., Harper, D.A.T., 2009. Ecostratigraphical interpretation of lower Middle Ordovician East Baltic sections based on brachiopods. Geol. Mag. 146, 717–731. https://doi.org/10.1017/S0016756809990148.
Rasmussen, C.M.Ø., Ullmann, C.V., Jakobsen, K.G., Lindskog, A., Hansen, J., Hansen, T., Eriksson, M.E., Dronov, A., Frei, R., Korte, C., Nielsen, A.T., Harper, D.A.T., 2016. Onset of main Phanerozoic marine radiation sparked by emerging Mid Ordovician icehouse. Sci. Rep. 6, 18884. https://doi.org/10.1038/srep18884.
Rasmussen, C.M.Ø., Kröger, B., Nielsen, M.L., Colmenar, J., 2019. Cascading trend of Early Paleozoic marine radiations paused by Late Ordovician extinctions. Proc. Natl. Acad. Sci. 116, 7207–7213. https://doi.org/10.1073/pnas.1821123116.
Read, J.F., 1980. Carbonate ramp-to-basin transitions and foreland basin evolution, middle Ordovician, Virginia Appalachians. AAPG Bull. 64, 1575–1612.
Read, J.F., 1982. Geometry, facies, and development of middle Ordovician carbonate buildups, Virginia Appalachians. AAPG Bull. 66, 189–209.
Rodgers, J., 1971. The Taconic orogeny. GSA Bull. 82, 1141–1178. https://doi.org/10.1130/0016-7606(1971)82[1141:TTO]2.0.CO;2.
Ronov, A.B., Khain, V.E., Balukhovsky, A.N., Seslavinsky, K.B., 1980. Quantitative analysis of Phanerozoic sedimentation. Sediment. Geol. 25, 311–325. https://doi.org/10.1016/0037-0738(80)90067-6.
Royer, D.L., Donnadieu, Y., Park, J., Kowalczyk, J., Goddéris, Y., 2014. Error analysis of CO_2 and O_2 estimates from the long-term geochemical model GEOCARBSULF. Am. J. Sci. 314, 1259–1283. https://doi.org/10.2475/09.2014.01.
Saltzman, M.R., Edwards, C.T., 2017. Gradients in the carbon isotopic composition of Ordovician shallow water carbonates: a potential pitfall in estimates of ancient CO_2 and O_2. Earth Planet. Sci. Lett. 464, 46–54. https://doi.org/10.1016/j.epsl.2017.02.011.
Saltzman, M.R., Thomas, E., 2012. Carbon isotope stratigraphy. In: The Geologic Time Scale. Elsevier, pp. 207–232.
Saltzman, M.R., Young, S.A., 2005. Long-lived glaciation in the Late Ordovician? Isotopic and sequence-stratigraphic evidence from western Laurentia. Geology 33, 109–112. https://doi.org/10.1130/G21219.1.
Saltzman, M.R., Edwards, C.T., Leslie, S.A., Dwyer, G.S., Bauer, J.A., Repetski, J.E., Harris, A.G., Bergström, S.M., 2014. Calibration of a conodont apatite-based Ordovician $^{87}Sr/^{86}$ Sr curve to biostratigraphy and geochronology: Implications for stratigraphic resolution. Geol. Soc. Am. Bull. 126, 1551–1568. https://doi.org/10.1130/B31038.1.
Scotese, C., 2014. Atlas of Silurian and Middle - Late Ordovician. The Early Paleozoic. PALEOMAP Atlas for ArcGIS.
Scotese, C.R., Wright, N., 2018. PALEOMAP paleodigital elevation models (PaleoDEMS) for the Phanerozoic. (PALEOMAP Proj).
Sell, B., Ainsaar, L., Leslie, S., 2013. Precise timing of the Late Ordovician (Sandbian) super-eruptions and associated environmental, biological, and climatological events.

J. Geol. Soc. 170, 711–714. https://doi.org/10.1144/jgs2012-148.
Sepkoski, J.J., 1995. The Ordovician radiations: diversification and extinction shown by global genus-level taxonomic data, in: Ordovician Odyssey: Short Papers for The Seventh International Symposium on The Ordovician System. SEPM (Society for Sedimentary Geology), pp. 393–396.
Servais, T., Harper, D.A.T., 2018. The Great Ordovician Biodiversification Event (GOBE): definition, concept and duration. Lethaia 51, 151–164. https://doi.org/10.1111/let.12259.
Shields, G.A., Mills, B.J.W., 2017. Tectonic controls on the long-term carbon isotope mass balance. Proc. Natl. Acad. Sci. 114, 4318–4323. https://doi.org/10.1073/pnas.1614506114.
Shields, G.A., Carden, G.A.F., Veizer, J., Meidla, T., Rong, J.-Y., Li, R.-Y., 2003. Sr, C, and O isotope geochemistry of Ordovician brachiopods: a major isotopic event around the Middle-Late Ordovician transition. Geochim. Cosmochim. Acta 67, 2005–2025. https://doi.org/10.1016/S0016-7037(02)01116-X.
Steiger, R.H., Jäger, E., 1977. Subcommission on geochronology: convention on the use of decay constants in geo- and cosmochronology. Earth Planet. Sci. Lett. 36, 359–362. https://doi.org/10.1016/0012-821X(77)90060-7.
Stigall, A.L., Edwards, C.T., Freeman, R.L., Rasmussen, C.M.Ø., 2019. Coordinated biotic and abiotic change during the Great Ordovician Biodiversification Event: Darriwilian assembly of early Paleozoic building blocks. Palaeogeogr. Palaeoclimatol. Palaeoecol. 530, 249–270. https://doi.org/10.1016/j.palaeo.2019.05.034.
Swanson-Hysell, N.L., Macdonald, F.A., 2017. Tropical weathering of the Taconic orogeny as a driver for Ordovician cooling. Geology 45, 719–722. https://doi.org/10.1130/G38985.1.
Swart, P.K., Oehlert, A.M., 2018. Revised interpretations of stable C and O patterns in carbonate rocks resulting from meteoric diagenesis. Sediment. Geol. 364, 14–23. https://doi.org/10.1016/j.sedgeo.2017.12.005.
Thompson, C.K., Kah, L.C., 2012. Sulfur isotope evidence for widespread euxinia and a fluctuating oxycline in Early to Middle Ordovician greenhouse oceans. Palaeogeogr. Palaeoclimatol. Palaeoecol. 313–314, 189–214. https://doi.org/10.1016/j.palaeo.2011.10.020.
Torsvik, T.H., Cocks, L.R.M., 2017. Earth History and Palaeogeography. Cambridge University Press, Cambridge. https://doi.org/10.1017/9781316225523.
Trotter, J.A., Williams, I.S., Barnes, C.R., Lécuyer, C., Nicoll, R.S., 2008. Did cooling oceans trigger Ordovician biodiversification? Evidence from conodont thermometry. Science 321, 550–554. https://doi.org/10.1126/science.1155814.
Wallace, M.W., Hood, A.vS., Shuster, A., Greig, A., Planavsky, N.J., Reed, C.P., 2017. Oxygenation history of the Neoproterozoic to early Phanerozoic and the rise of land plants. Earth Planet. Sci. Lett. 466, 12–19. https://doi.org/10.1016/j.epsl.2017.02.046.
Webby, B.D. (Ed.), 2004. The Great Ordovician Biodiversification Event, Critical Moments and Perspectives in Earth History and Paleobiology. Columbia University Press, New York.
Young, S.A., Saltzman, M.R., Bergström, S.M., 2005. Upper Ordovician (Mohawkian) carbon isotope ($\delta^{13}C$) stratigraphy in eastern and central North America: Regional expression of a perturbation of the global carbon cycle. Palaeogeogr. Palaeoclimatol. Palaeoecol. 222, 53–76. https://doi.org/10.1016/j.palaeo.2005.03.008.
Young, S.A., Saltzman, M.R., Foland, K.A., Linder, J.S., Kump, L.R., 2009. A major drop in seawater $^{87}Sr/^{86}Sr$ during the Middle Ordovician (Darriwilian): links to volcanism and climate? Geology 37, 951–954. https://doi.org/10.1130/G30152A.1.
Young, S.A., Gill, B.C., Edwards, C.T., Saltzman, M.R., Leslie, S.A., 2016. Middle–Late Ordovician (Darriwilian–Sandbian) decoupling of global sulfur and carbon cycles: isotopic evidence from eastern and southern Laurentia. Palaeogeogr. Palaeoclimatol. Palaeoecol., The Ordovician Revolution: Co-Evolution of Climate and the Biosphere 458, 118–132. doi:https://doi.org/10.1016/j.palaeo.2015.09.040.
Zhang, S., Planavsky, N.J., Krause, A.J., Bolton, E.W., Mills, B.J.W., 2018. Model based Paleozoic atmospheric oxygen estimates: a revisit to GEOCARBSULF. Am. J. Sci. 318, 557–589. https://doi.org/10.2475/05.2018.05.